Terahertz radiation due to random grating coupled surface plasmon polaritons

T. V. Shubina,[1] N. A. Gippius,[2,3] V. A. Shalygin,[4] A. V. Andrianov,[1] and S. V. Ivanov[1]
[1]*Ioffe Physico-Technical Institute, RAS, St. Petersburg 194021, Russia*
[2]*LASMEA, UMR 6602, Universite Blaise Pascal, FR-63177 Aubiere Cedex, France*
[3]*General Physics Institute RAS, Moscow 119991, Russia*
[4]*St. Petersburg State Polytechnical University, St. Petersburg 195251, Russia*
(Received 13 November 2010; revised manuscript received 20 January 2011; published 18 April 2011; corrected 3 May 2011)

We report on terahertz (THz) radiation under electrical pumping from a degenerate semiconductor possessing an electron accumulation layer. In InN, the random grating formed by topographical defects provides high-efficiency coupling of surface plasmon polaritons, supported by the accumulation layer, to the THz emission. The principal emission band occupies the spectral range of 2–6 THz. We establish a link between the shape of emission spectra and the structural factor of the random grating and show that the change of slope of power dependencies is characteristic for temperature-dependent plasmonic mechanisms. The super-linear rise of a THz emission intensity on applied electric power provides the advantage of such materials in emission yield.

DOI: 10.1103/PhysRevB.83.165312 PACS number(s): 73.20.Mf

I. INTRODUCTION

The surface plasma waves confined to the interface between a conductor (metal or degenerate semiconductor) and a dielectric attract a lot of attention for terahertz (THz) frequency range application.[1–3] The characteristic frequency of a surface plasmon at the sharp interface of the semi-infinite conductor with a bounding medium is given by

$$\omega_s^2 = 4\pi N e^2/m^*(\varepsilon + \varepsilon_b), \tag{1}$$

where N, e, and m^* are the bulk concentration, charge, and effective mass of carriers in the conductor, and ε and ε_b are the dielectric constants of the conducting and bounding media, respectively. For an ideal metal bounded by vacuum, Eq. (1) is simplified as $\omega_s^2 = 2\pi N e^2/m^*$. The frequency is in the visible range for the metals, being in the mid-infrared and even in the terahertz ranges for the degenerate semiconductors.[2,4–6]

The distinct difference between these two materials is that the interband absorption in the metals[7] can hamper strong plasmonic resonances at optical frequencies, while in the semiconductors they are much below an absorption edge. In general, the strong resonances arise when the ratio of the real to imaginary part of the complex dielectric function markedly exceeds unity.[8] As a result, the pronounced plasmonic effects in metallic structures,[9,10] as well as the long propagation length of surface plasmon polaritons,[11] have been usually observed below the interband absorption range. It is worth noting that, to maintain surface plasmon polariton modes, the special conditions must be fulfilled. The detailed analysis of these with symmetrical and asymmetrical surroundings can be found, e.g., in Ref. 12.

Ritchie[13] first noted that the plasmon frequency of a thin sheet of carriers has a square-root dependence on the plasmon wave vector k. Later, Stern[14] derived the explicit dispersion relation, which (for large enough values of k) can be written as $\omega^2 = k(2\pi N_s e^2/m^*\varepsilon_b)$, where N_s is the number of electrons per unit area. (This relation is more complicated for plasmons in the films of a finite thickness.[12,15,16]) It determines why the surface plasmons can not radiate to ambience directly. Their wave vector is always larger than that of light, $k_0 = \omega/c$, at the same frequency. Coupling of the plasmon with an electromagnetic wave occurs by means of the momentum exchange either at the disturbances induced by plasma wave instability[1] or at the periodical modulations of surface profile.[2,4,5] At $k \gg k_0$, the radiating states have the momentum $k \approx 2\pi m/a$ ($m = 1,2,\ldots$), where a is a grating period.

In the case of the ideal grating, the k intervals where the emission yield takes place are inevitably narrow and the integral emission intensity is sometimes not sufficient. An example of an emission spectrum with a set of very narrow lines, the sequence of which is coordinated with an average grating period, has been recently published in Ref. 17. The spectrum was recorded from an InN layer, where the grating is formed by defects situated with a certain periodicity. To expand radiation bands, more complicated (multiple-section) gratings are usually exploited.[18–20] Note that the observed advantage at certain conditions of InN layers in emitting power with respect to other structures[17] has not been explained yet.

In this paper, we show that random grating can effectively couple surface plasmon polaritons in degenerate semiconductors with radiation in a spectral range as wide as several THz. We analyze the shapes of the THz spectra at the random grating and describe the power dependencies characteristic of the plasmonic mechanism at electrical pumping. Our studies elucidate how the population of plasmonic states with increasing electron temperature influences the emission process in the presence of the random grating, which breaks down equilibrium in plasmon momentum distribution. This is complemented by data on electron-surface-plasmon aloof scattering as an evidence of the surface plasmon polaritons.

II. EXPERIMENTAL DETAILS AND REQUIREMENTS TO A PLASMON SUPPORTING LAYER

This study has been done using InN epilayers where the random grating is formed by topographic defects. We have chosen the epilayers, each of which has had one type of dominant defect, such as nanocolumns, trenches, pores, or metallic clusters. It has allowed us to discover the general features, which are not dependent on the defect type.

The (1–3)-μm-thick InN epilayers with unintentional electron concentrations of 10^{18}–10^{19} cm^{-3} were grown at 450°–550° C by plasma-assisted molecular beam epitaxy on c-sapphire atop of GaN buffers. The distances between the defects varies in the (0.1–1)-μm range. The THz spectra were measured at 8 K using a step-scan Fourier spectrometer with excitation by series of packets of 15-V rectangular pulses of 10-μs duration separated by 10-μs time interval (the repetition rate of the pulse packets was 71.5 Hz). Such a bias was used to minimize the effect of lattice heating. The dependencies of integral THz emission intensity on the electric power were measured at 4.2 K using 2-μs-long pulses and a Ge:Ga photodetector with the (2.3–6.4)-THz spectral sensitivity range. The samples exhibited spontaneous emission with frequencies in the range of several terahertz (10–40 meV), i.e., below the characteristic energies of surface phonon excitations [$\sim$60 meV (Ref. 21)]. The dissected spectra of the emission have nothing in common with broadband THz radiation observed earlier using optical excitation by ultrashort laser pulses.[22,23]

Calculations based on numerical solving of the Maxwell equations for multiple-layer structures have been used as the first step to model the full set of plasmonic and waveguide modes supported in the studied samples and to choose the thickness range suitable for the experimentally observed frequency of emission. This modeling has demonstrated that the layer thickness d must be rather small to provide the coupling by the typical InN defects at the experimentally observed emission frequencies. This result is consistent with other requirements $kd \ll 1$ needed to support the long propagating surface modes.[12,15,16]

For the sake of demonstration, we present in Fig. 1 the plasmon dispersion curves calculated for different thicknesses using the simplified three-layer model,[16,17] where the metal-like layer of thickness d ($N = 10^{19}$ cm^{-3}, $m^* = 0.13m_0$) is

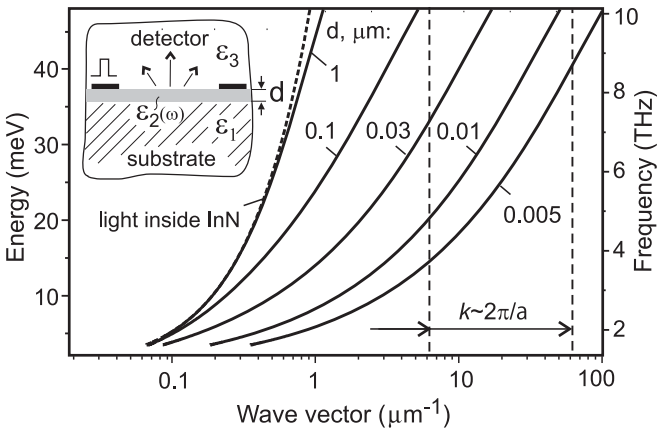

FIG. 1. Dispersion dependencies (semilogarithmic scale) calculated for the different thicknesses d of a layer, where plasmon propagates, shown together with the light wave dispersion inside InN. The crossing of vertical dashed lines with plasmon dispersion curves indicates the d thickness range suitable for the first-order coupling ($k \sim 2\pi/a$) with $a = 0.1 \div 1$ μm. The inset presents schematically a studied sample with contacts on the top. It contains the metal-like layer, characterized by the complex dielectric function $\varepsilon_2(\omega)$, situated between the rest structure (ε_1) and vacuum (ε_3).

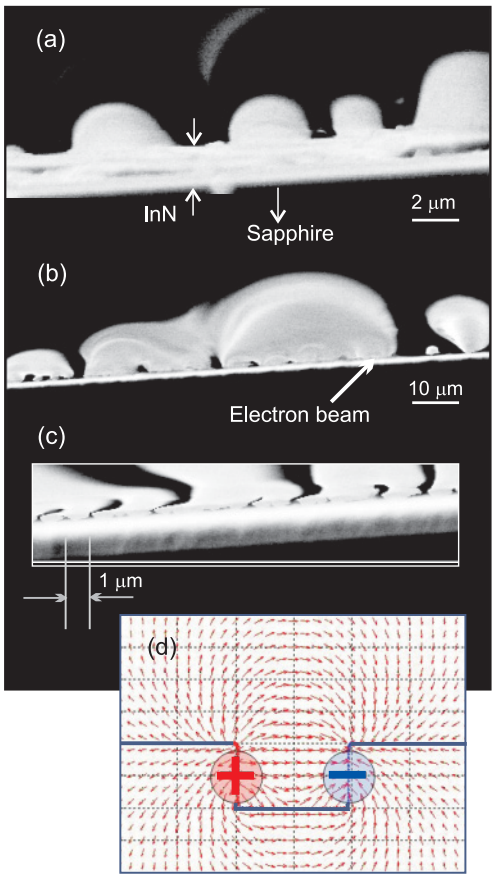

FIG. 2. (Color online) (a) SE SEM image taken at the beginning of electron beam exposure. (b) Image taken 20 minutes after exhibits growing and overlapping of the SE clouds with the exposure time. The lower magnification is used to display the full picture. (c) Image taken from a sample detuned slightly to show discretion in a cloud base. (d) Calculated distribution of electric field vectors around a charged pit.

placed between the vacuum and the rest of the InN epilayer, which is considered as a dielectric (see Fig. 1, inset). The Drude model with damping parameter of 1 meV was used to describe the complex dielectric function of this thin layer. The static permittivity of 14 has been accepted for InN.[24] Temperature effects, weak in InN,[25] are neglected. The calculations show that the coupling is possible if the thickness of the layer does not exceed tens of nanometers. A good candidate for this is a surface electron accumulation layer, existing in n-doped semiconductors.[26–28] The presence of the layer in InN with thickness of 4–10 nm has been previously confirmed by the spectroscopy of electron energy losses induced by surface plasma waves.[21,25]

III. ELECTRON-SURFACE-PLASMON ALOOF SCATTERING

The electron beam excitation is a very efficient way to create surface plasmons.[29] The scanning electron microscopy (SEM) studies of our samples have permitted us to observe phenomena related presumably to the surface plasmon polaritons in the accumulation layer. The SEM studies were performed with

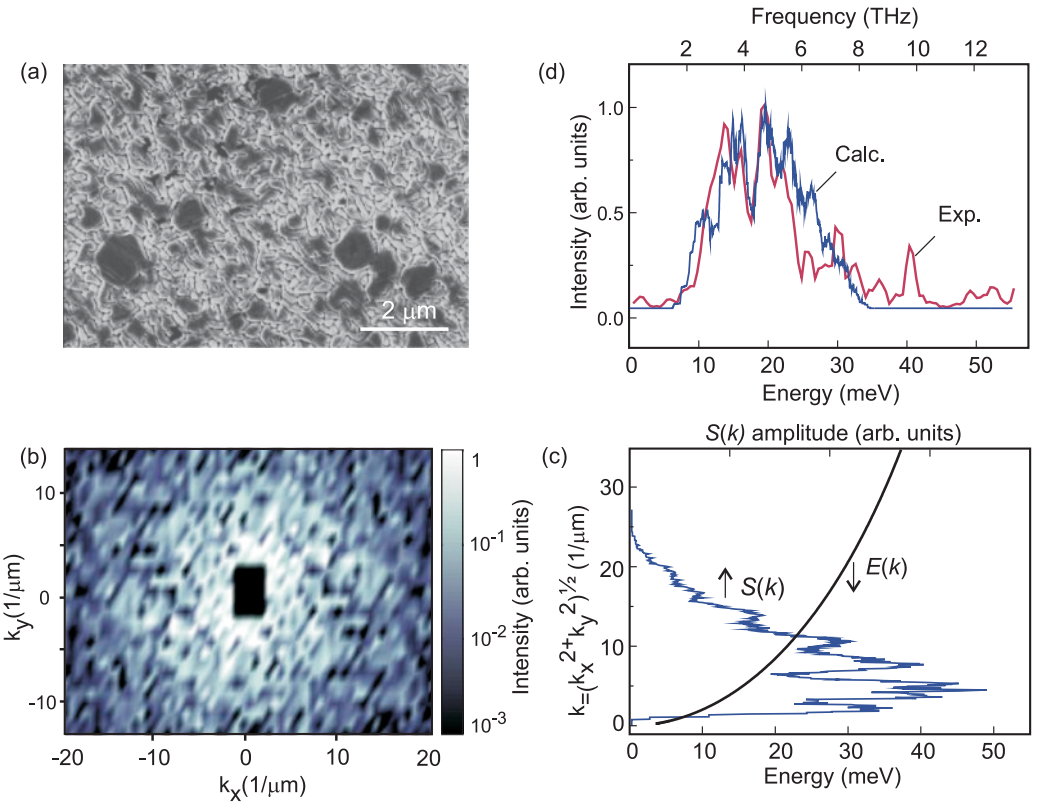

FIG. 3. (Color online) (a) SEM image of a surface of an InN epilayer (sample A). (b) Image of the structural factor of random grating obtained by the Fourier transformation of the SEM image. (c) The correlation between the plasmon dispersion $E(k)$ and the structural factor $S(k)$. (d) Comparison of calculated and experimental spectra. (See text for details.)

an electron beam impinging normally to a cleaved facet of a layer. This configuration corresponds to the so-called aloof scattering, when the electrons moving along the nontouching trajectory can stimulate plasmons in conductors due to image potential. The nonradiative decay of the plasmons results in the generation of secondary electrons (SEs).[30–32]

The SEM images recorded from the sample facets display intricate features, clouds above the sample surface, which have a specific semispherical shape (Fig. 2). Their sizes are increasing with the time of exposure to the electron beam [compare, e.g., Figs. 2(a) and 2(b) taken with the interval of 20 min]. With a slight declining of a sample, a discrete base of the clouds can be resolved [Fig. 2(c)]. The step in the base is approximately equal to the average distance between the topographic defects. We believe that these clouds are formed by the SEs generated during the plasmon decay and, probably, by a part of the scattered electrons.

The strength of the aloof scattering is strongest near the turning point of the parabolic trajectory. It goes down with increasing distance z from the surface. However, it has been shown[31] that it is significant up to $z \sim 3/k$, which amounts to microns in our case. The surface roughness dominates this scattering at small z, especially when the ratio of the average depth of inhomogeneities to the mean distance between them tends to unity.[33]

The plasmon excitation in the aloof mode implies that the defects scatter the electrons comprising the electron beam.[30] Consecutive charge accumulation takes place, similar to that under the exposure to plasma.[34] Figure 2(d) presents the calculated distribution of the electric field vectors at a pit, bearing a dipole charge. It resembles a pattern of a separated cloud. This permits us to suggest that the electrons depict an electric field around the charged defect in the same way as the iron filings display the magnetic field lines.

This observation was done using InN samples exhibiting THz emission. As a rule, the stronger the emission intensity was, the more pronounced clouds were observed. (The quantitative relationship between them can hardly be established due to the strongly different ways of excitation.) It is worth noting that SEs can escape from a rather small depth of several nanometers. This value is well consistent with the thickness of a surface-electron accumulation layer.

IV. EMISSION SPECTRA AT RANDOM GRATING

To consider the spectra of the terahertz emission from the InN epilayers, we assume first that surface plasmons are translated to the light cone by spatial harmonics of the random grating preserving the frequency given by the plasmon dispersion. To find the structural factor of the random grating $S(k)$, the Fourier transformation of a SEM image was performed using the two-dimensional discrete fast Fourier transform algorithm. In the Fourier domain image, each point represents a particular k harmonic contained in the spatial domain image.

The amplitude of the harmonics in this point reflects its weight. Figures 3(a) and 3(b) demonstrate this transformation performed for the sample A, where the dominant defects are narrow intercolumn trenches. The Fourier image [Fig. 3(b)] is rearranged in a standard way by moving the zero-frequency component to the center of the array. The color scale gives the intensity range of the harmonic amplitudes. The dark spot in the center is due to removing the unnecessary harmonics of lowest orders, which appear due to finite size of the SEM image.

In further calculations, the harmonic amplitudes are considered as a function of $k = \sqrt{k_x^2 + k_y^2}$. Such a $S(k)$ spectrum in arbitrary units is shown in Fig. 3(c) together with the plasmon dispersion, calculated as described in Sec. II with $d = 7$ nm. Then, it is quite reasonable to suggest that the intensity of the radiation at certain energy is proportional to the amplitude of the respective harmonic. The influence of the plasmon dispersion is taken into account by multiplying on the plasmon density of states in this point. Such an approach permits us to simulate directly an emission spectrum, neglecting higher-order scattering. Figure 3(d) demonstrates the good agreement between the computed and experimental spectra, in spite of a rather complicated shape provided by the random grating.

In accord with the energy and momentum conservation requirements, the higher-energy electrons populate plasmonic states with lower k vectors.[35] In our calculations, we ignore such a nonequilibrium plasmon population that provides, likely, some underestimation of the intensity of the lower-energy peaks in the calculated spectrum. In particular, it can provide the shift of the lower-energy maximum to 15 meV in the calculated emission spectrum, while it takes place at 13 meV in the experimental one. The other difference concerns the higher-energy cutoff of the main emission band, which is at 32 meV versus 23 meV in the calculated and experimental spectra, respectively. This difference arises out of disregarding the finite population of the plasmonic states.

At electrical pumping, the filling level is controlled by the electron temperature T, which can markedly exceed the lattice temperature.[2,36] Its value is roughly proportional to the electrical power P_{el}. Our spectral measurements were done using a spared regime, corresponding to the average electron temperature ~10–20 K. The complete filling of all possible plasmonic states in the sample A, e.g., would be at 35 K. Thus, the actual filling level was lower than the energy corresponding to the largest $k^{\max}$ in the grating wave-vector distribution.

V. POWER DEPENDENCIES

The filling effect influences also the dependencies of emission intensity on electric power, namely, their characteristic slopes. To describe this, we suppose the plasmons to be thermalized with temperature T, e.g., via the electron scattering by phonons, impurities, and other defects.[36,37] The emitting power $W(T)$ can be estimated by integration over

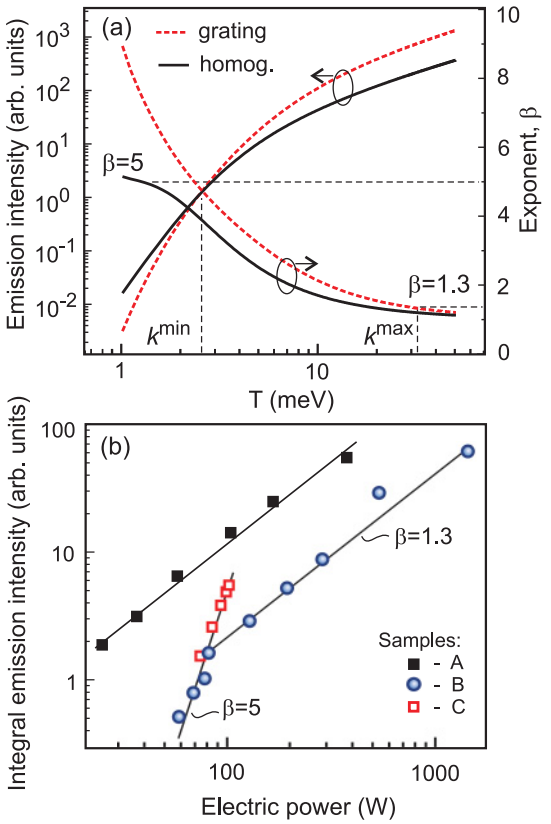

FIG. 4. (Color online) (a) Dependencies of the emission intensity on temperature (given in energy units) calculated for the homogeneous filling of plasmon states and for the filling of grating coupled states. The vertical lines mark the interval corresponding to the occupation of the grating coupled states in the sample A. (b) Experimental dependencies of the emission intensity on the electrical power of representative samples exhibiting the similar slopes and the kink between them. The lines $\beta = 5$ and 1.3 are given as a guide to the eye.

all plasmon states with the energy $E(k)$, occupation of these states, and the structural factor of the grating $S(k)$:

$$W(T) = \int k\,dk\,S(k)E(k)/\{\exp[E(k)/T] - 1\}. \quad (2)$$

Here, the temperature T is given in the energy units. Two following limiting cases are considered: (i) homogeneous emission from all possible plasmon states assuming $S(k) =$ const and (ii) emission from the grating coupled states with $S(k)$ derived from the SEM image (presented, e.g., in Fig. 3).

The performed calculations show that the mechanism based on the uniform scattering dominates when $T \leqslant E(k^{\min})$, i.e., when the states corresponding to the minimal grating wave vector are not populated yet [Fig. 4(a)]. Consequently, the slope in the resulting emission power dependency must have the exponent $\beta \sim 5$. (This T^5 law appears due to the superposition of the Planck distribution function and the plasmon dispersion.) With the T rise, the mechanism of the emission changes; now most of the emission comes from the plasmons interacting with the random grating. When the temperature approaches the higher-energy cutoff $T \sim E(k^{\max})$, the $\beta \sim 1.3$ is expected. The predicted slopes and their change are observed in the experimental dependencies of the radiated intensity on

the electric power [Fig. 4(b)]. The distinctiveness of the kink and the corresponding P_{el} value are specific for each sample, being dependent on the grating pattern and plasmon dispersion.

For the sake of clarity, the presented consideration is markedly simplified. Nevertheless, it displays the basic features of the plasmonic emission. In particular, the superlinear rise of the InN THz intensity with increasing electric power ($\beta \geqslant 1.3$) prevails over sublinear laws inherent to other processes in semiconductor structures.[17] It results in the emission from InN with the density (for the 2π solid angle) as high as 30 μW/cm^2 in the (2–6)-THz spectral range.

VI. CONCLUDING REMARKS

In general, our studies show that surface plasmon polaritons can be the origin of THz emission from degenerate semiconductors, such as InN, InAs, and InSb, where an electron accumulation layer is modulated by structural inhomogeneities. The THz emission appears in the spectral range determined by both grating structural factor and plasmon dispersion. A similar mechanism is anticipated for intentionally formed gratings. Our findings may have important practical applications for the creation of effective terahertz emitters.

ACKNOWLEDGMENTS

We thank M. I. Dyakonov for fruitful discussions; V. N. Jmerik and A. M. Mizerov for sample growth; A. O. Zakhar'in and A. N. Sofronov for the help in THz studies; and A. Yoshikawa and W. Schaff for supplying reference samples. This work was supported in part by the RFBR and the Program of the Presidium of RAN.

[1] M. I. Dyakonov and M. S. Shur, Phys. Rev. Lett. **71**, 2465 (1993).
[2] R. A. Höpfel, E. Vass, and E. Gornik, Phys. Rev. Lett. **49**, 1667 (1982).
[3] M. Dragomana and D. Dragoman, Prog. Quantum Electron. **32**, 1 (2008).
[4] S. J. Allen, D. C. Tsui, and R. A. Logan, Phys. Rev. Lett. **38**, 980 (1977).
[5] J. Gómez Rivas, M. Kuttge, P. Haring Bolivar, H. Kurz, and J. A. Sánchez-Gil, Phys. Rev. Lett. **93**, 256804 (2004).
[6] W. E. Anderson Jr., R. W. Alexander, and R. J. Bell, Phys. Rev. Lett. **27**, 1057 (1971).
[7] P. B. Johnson and R. W. Christy, Phys. Rev. B **6**, 4370 (1972).
[8] T. V. Shubina, V. A. Kosobukin, T. A. Komissarova, V. N. Jmerik, A. N. Semenov, B. Ya. Meltser, P. S. Kop'ev, S. V. Ivanov, A. Vasson, J. Leymarie, N. A. Gippius, T. Araki, T. Akagi, and Y. Nanishi, Phys. Rev. B **79**, 153105 (2009).
[9] C. Genet and T. W. Ebbesen, Nature (London) **445**, 39 (2007).
[10] A. A. Toropov, T. V. Shubina, V. N. Jmerik, S. V. Ivanov, Y. Ogawa, and F. Minami, Phys. Rev. Lett. **103**, 037403 (2009).
[11] J. T. van Wijngaarden, E. Verhagen, A. Polmana, C. E. Ross, H. J. Lezec, and H. A. Atwater, Appl. Phys. Lett. **88**, 221111 (2006).
[12] F. Yang, J. R. Sambles, and G. W. Bradberry, Phys. Rev. B **44**, 5855 (1991).
[13] R. H. Ritchie, Phys. Rev. **106**, 874 (1957).
[14] F. Stern, Phys. Rev. Lett. **18**, 546 (1967).
[15] E. N. Economou, Phys. Rev. **182**, 539 (1969).
[16] J. J. Burke, G. I. Stegeman, and T. Tamir, Phys. Rev. B **33**, 5186 (1986).
[17] T. V. Shubina, A. V. Andrianov, A. O. Zakhar'in, V. N. Jmerik, I. P. Soshnikov, T. A. Komissarova, A. A. Usikova, P. S. Kop'ev, S. V. Ivanov, V. A. Shalygin, A. N. Sofronov, D. A. Firsov, L. E. Vorob'ev, N. A. Gippius, J. Leymarie, X. Wang, and A. Yoshikawa, Appl. Phys. Lett. **96**, 183106 (2010).
[18] Y. M. Meziani, H. Handa, W. Knap, T. Otsuji, E. Sano, V. V. Popov, G. M. Tsymbalov, D. Coquillat, and F. Teppe, Appl. Phys. Lett. **92**, 201108 (2008).
[19] R. J. Wilkinson, C. D. Ager, T. Duffield, H. P. Hughes, D. G. Hasko, H. Ahmed, J. E. F. Frost, D. C. Peacockl, D. A. Ritchie, G. A. C. Jones, C. R. Whitehouse, and N. J. Apsley, J. Appl. Phys. **71**, 6049 (1992).
[20] T. Otsuji, Y. M. Meziani, M. Hanabe, T. Ishibashi, T. Uno, and E. Sano, Appl. Phys. Lett. **89**, 263502 (2006).
[21] I. Mahboob, T. D. Veal, C. F. McConville, H. Lu, and W. J. Schaff, Phys. Rev. Lett. **92**, 036804 (2004).
[22] R. Ascázubi, I. Wilke, K. Denniston, H. Lu, and W. J. Schaff, Appl. Phys. Lett. **84**, 4810 (2004).
[23] B. Pradarutti, G. Matthäus, C. Brückner, S. Riehemann, G. Notni, S. Nolte, V. Cimalla, V. Lebedev, O. Ambacher, A. Tünnermann, Proc. SPIE **6194**, 61940I (2006).
[24] V. Yu. Davydov, V. V. Emtsev, I. N. Goncharuk, A. N. Smirnov, V. D. Petrikov, V. V. Mamutin, V. A. Vekshin, and S. V. Ivanov, Appl. Phys. Lett. **75**, 3297 (1999).
[25] L. F. J. Piper, T. D. Veal, I. Mahboob, C. F. McConville, H. Lu, and W. J. Schaff, Phys. Rev. B **70**, 115333 (2004).
[26] C. C. Kao and E. M. Conwell, Phys. Rev. B **14**, 2464 (1976).
[27] G. R. Bell, C. F. McConville, and T. S. Jones, Phys. Rev. B **54**, 2654 (1996).
[28] D. H. Ehlers and D. L. Mills, Phys. Rev. B **36**, 1051 (1987).
[29] F. J. Garcia de Abajo, Rev. Mod. Phys. **82**, 210 (2010).
[30] R. J. Warmack, R. S. Becker, V. E. Anderson, R. H. Ritchie, Y. T. Chu, J. Little, and T. L. Ferrell, Phys. Rev. B **29**, 4375 (1984).
[31] J. Lecante, Y. Ballu, and D. M. Newns, Phys. Rev. Lett. **38**, 36 (1977).
[32] M. S. Chung and T. E. Everhart, Phys. Rev. B **15**, 4699 (1977).
[33] T. S. Rahman and A. A. Maradudin, Phys. Rev. B **21**, 504 (1980).
[34] G. S. Upadhyaya, J. L. Shohet, and J. B. Kruger, Appl. Phys. Lett. **91**, 182108 (2007).
[35] V. V. Popov and T. Yu. Bagaeva, Phys. B (Amsterdam) **269**, 290 (1999).
[36] R. Z. Vitlina and A. V. Chaplik, Zh. Eksp. Teor. Fiz. **83**, 1457 (1982) [Sov. Phys. JETP **56**, 839 (1982)].
[37] M. Richter, S. Butscher, M. Schaarschmidt, and A. Knorr, Phys. Rev. B **75**, 115331 (2007).